SLAC Technical Note: ***SLAC-TN-10-026***

Resource Letter on Stimulated Inelastic X-ray Scattering at an XFEL

Bruce D Patterson*

SLAC National Accelerator Laboratory, Menlo Park, CA 94025, USA
and
Paul Scherrer Institut, CH-5232 Villigen, Switzerland

At sufficient X-ray intensity, stimulated effects in inelastic scattering will become important. These coherent, non-linear optical phenomena may be used to impulsively produce a high degree of collective excitation in, for example, correlated electron materials, suitable for performing ultrafast time-resolved spectroscopy. This Resource Letter collects information on fundamental aspects of stimulated X-ray scattering and evaluates the prospect for successful experiments at a present or future X-ray free electron laser (XFEL) facility.

Introduction

Conventional resonant inelastic X-ray scattering (RIXS) [1,2] is a synchrotron-based, photon-in photon-out, chemically-specific spectroscopic method which allows the study in solids of, *e.g.*, d-d, charge-transfer and collective excitations [3,4,5], without the limitations of probing depth, low ambient EM-fields, sample conductivity and surface quality presented by photoemission. In spite of resonance enhancement, the main drawback of RIXS is its low efficiency, generally 10^{-5} of elastic Rayleigh scattering, implying that a typical spectral measurement requires several days at a third generation undulator beamline. This low efficiency effectively precludes the possibility at a synchrotron of time-dependent, pump-probe RIXS measurements.

Like its Raman scattering optical analog, the RIXS technique relies on *spontaneous* emission from a photo-excited state to produce the observed outgoing photon. At sufficiently high incoming photon fluence, the efficiency of *stimulated* Raman scattering exceeds that of the spontaneous process, with gains in efficiency at optical wavelengths of up to 10^7. And using ps and fs optical pulses, a variety of techniques have been devised of performing *time-dependent* stimulated Raman scattering, some of which make explicit use of the large bandwidth of the exciting radiation, and the majority of which require multi-color pulses.

With the advent at the Linear Coherent Light Source (LCLS) [6] of fs X-ray pulses with extreme peak brightness, and perhaps in the near future at the LCLS-II of multi-color pulse capabilities [7], it is interesting to consider the feasibility of time-resolved, non-linear X-ray spectroscopy. This Letter begins by making the distinction between spontaneous and stimulated RIXS and highlighting the importance of the third-order susceptibility $\chi^{(3)}$ in these and related processes. Using a simple model, estimations are made of $\chi^{(3)}$ at optical and X-ray wavelengths, which are then used to compute cross-sections for stimulated scattering and optical pumping. Next, an impulsive method is presented where a single pulse delivers both of the frequency components

Work supported in part by US Department of Energy contract DE-AC02-76SF00515.

required for stimulated scattering. The relative probability of spontaneous and stimulated scattering is determined by the source degeneracy - the number of photons per radiation mode, and values are given for various optical and X-ray sources. Three proposals for performing non-linear, time-dependent X-ray spectroscopy are then discussed, emphasizing the distinction between homodyne and heterodyne detection and the importance of phase-matching. The Letter closes with recommendations for initial experiments at an XFEL based on the transient grating spectroscopic method.

Selected light-matter interactions

Our principal goal is to use chemically-specific resonant X-rays ($\hbar\omega = 0.5 - 10$ keV) to probe low-lying ($\hbar\Omega = 0.05 - 5$ eV) excitations in solids. The *direct* photo-excitation of a low-lying transition, loosely denoted *IR-absorption*, is possible in a sample if the electric dipole operator μ joins the ground state g and a low-level excited state f (Fig. 1a). We assume that the state f is long-lived (ns).

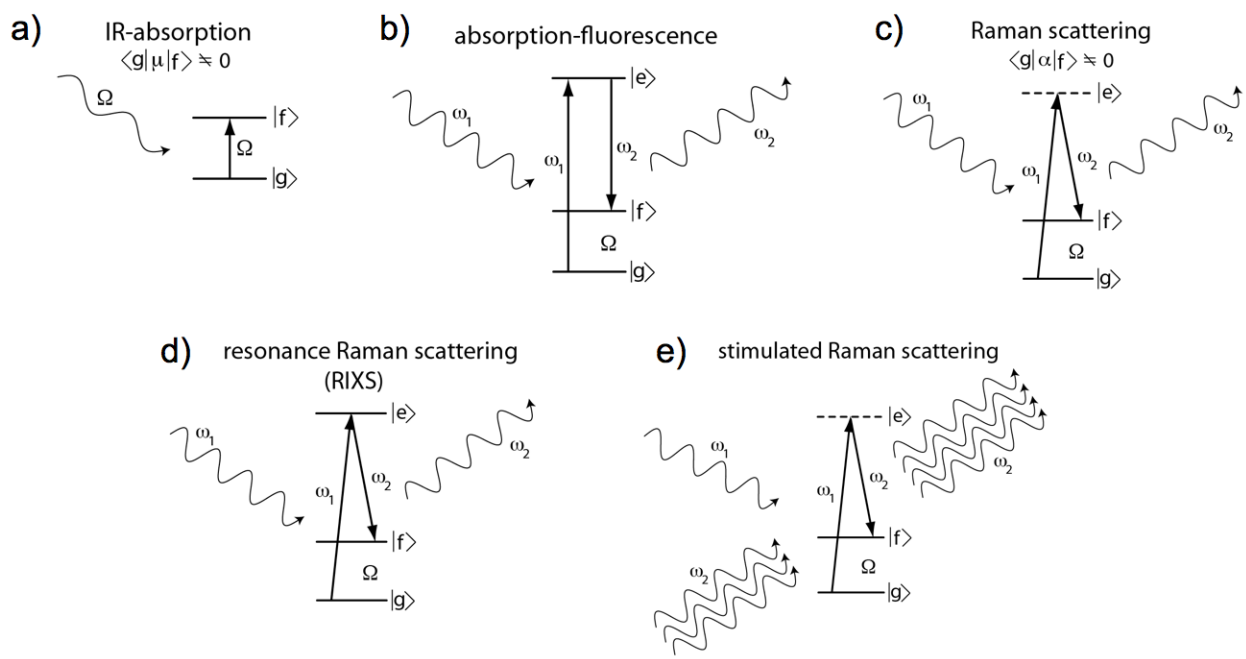

Figure 1. Schematic representations of selected light-matter interactions. See the text for explanations.

With short wavelength radiation ω_1, one can resonantly excite a higher-lying state e and observe the subsequent radiative decay ω_2 (fluorescence) to the state f (Fig. 1b). Using X-rays to excite, the intermediate state is a short-lived (5-10 fs) core-hole, and the principal competitor to fluorescence decay is the emission of an Auger electron. A small fraction of the optical photons incident on a sample may undergo inelastic, Raman scattering (Fig. 1c). Provided the electric polarizability α joins the states g and f, this effectively instantaneous single-step process emits the outgoing inelastic *Stokes* photon ω_2. Raman scattering is described classically in terms of the third-order susceptibility $\chi^{(3)}$ and quantum-mechanically using the Kramers-Heisenberg

formalism [8]. For the cases 1b-1c, a spectral measurement of the outgoing radiation yields the low-lying excitation energy $\hbar\Omega = \hbar\omega_1 - \hbar\omega_2$.

Enhanced sensitivity results when the incoming ω_1 photon is resonant with a true excited state transition $g \rightarrow e$ (Fig. 1d). In the optical regime, this is termed *resonance Raman scattering*, the optical analog of RIXS. Finally, if besides ω_1, a sufficiently large fluence of incident ω_2 photons is present, stimulated, rather than spontaneous, decay of the intermediate state *e* predominates, coherently amplifying the wavefield ω_2 via Raman gain [9]. Note that there is no threshold for stimulated Raman scattering.

Non-linear optics considerations

Spontaneous and stimulated Raman scattering, as well as other light-matter interactions to be discussed below, are examples of non-linear optical sprectroscopies, and these are divided into two categories [10,11]:

a) A *parametric* (*p*) process, also called *passive* or *elastic*, leaves the material properties unchanged, if one disregards a small energy dissipation in the intermediate state. The material thus acts as a catalyst for a change in the radiation fields.
b) In a *non-parametric* (*np*) process, also called *active* or *inelastic*, the material undergoes a large energy loss to or gain from the radiation field.

The interaction of a polarizable material with a varying electric field produces a time-dependent electric polarization, which can be expanded as a power series in the field strength:

$$\begin{aligned} P(t) &= \varepsilon_0 \left[\chi^{(1)} E(t) + \chi^{(2)} E^2(t) + \chi^{(3)} E^3(t) + \ldots \right] \\ &\equiv P^{(1)}(t) + P^{(2)}(t) + P^{(3)}(t) + \ldots \end{aligned} \tag{1}$$

For a superposition of light waves, where the electric field consists of several oscillating components, the non-linear terms in the polarization mix contributions with different frequencies, and the resulting Fourier components of the polarization are expressed in terms of the frequency-dependent non-linear susceptibilities $\chi^{(s)}$:

$$P^{(s)}(\omega_k) = \varepsilon_0 \chi^{(s)}(\omega_k = \omega_1 + \omega_2 + \ldots + \omega_s) E(\omega_1) \ldots E(\omega_s) \tag{2}$$

where the frequency ω_k can be any algebraic sum of the (positive and negative) frequencies which are active in the interaction.

The source term for parametric processes of any order is proportional to the corresponding susceptibility, and the cross-section for a non-parametric process is proportional to the *imaginary part* of an odd-order susceptibility times the modulus squared of each field involved. Non-parametric interactions thus require the presence of a nearby resonance. Materials with inversion symmetry have a vanishing second-order susceptibility. Examples of light-matter interactions are:

a) 1st order *np*: single-photon absorption or emission
b) 1st order *p*: light propagation with linear dispersion
c) 2nd order *p*: second-harmonic generation
d) 3rd order *np*: spontaneous and stimulated Raman scattering, governed by $\chi^{(3)}\left(\omega_2 = \omega_2 + \omega_1 - \omega_1\right)$
e) 3rd order *p*: four-wave mixing, and in particular, coherent anti-Stokes Raman scattering (CARS), governed by $\chi^{(3)}\left(\omega_s = \omega_1 - \omega_2 + \omega_1\right)$

Estimation of $\chi^{(3)}$

Third-order processes are of primary interest in this Letter. In order to obtain an order of magnitude for $\chi^{(3)}$, we make use of the centro-symmetric anharmonic oscillator model presented by Boyd [10]. For the electronic Raman scattering case, the model gives:

$$\chi^{(3)}\left(\omega_2 = \omega_2 + \omega_1 - \omega_1\right) / N \approx \frac{e^4\omega_0^2}{\varepsilon_0 m^3 r_a^2}\left(\frac{1}{\omega_0^2 - \omega_2^2 - 2i\gamma\omega_2}\right)^2 \left|\frac{1}{\omega_0^2 - \omega_1^2 - 2i\gamma\omega_1}\right|^2 \qquad (3)$$

where e and m are the electron charge and mass, respectively, r_a is the atomic radius, ω_0 is the resonance frequency and γ is the resonance linewidth. Boyd uses this formula to estimate the non-resonant susceptibility at optical wavelengths. By assuming that γ, ω_1, $\omega_2 << \omega_0$, and taking $\hbar\omega_0 = 4.6$ eV, $N = 3.7 \times 10^{22}$ cm^{-3} and $r_a = 3$ Å, he obtains the value $\chi_{nr,\,opt} \approx 0.34 \times 10^{-21}$ m^2/V^2.

Measured values of the non-resonant $\chi^{(3)}$ for various materials at optical wavelengths are also given by Boyd, and one finds suprisingly good agreement with the simple model (see Table 1). Also in the Table, the measurements have been divided by an assumed atomic density $N = 10^{22}$ cm^{-3} and converted [10] to Gaussian units ($\chi^{(3)}$ (Gaussian) = $[(100 \times 299.8)^2/4\pi]$ $\chi^{(3)}$ (MKS); 1 statvolt = 299.8 V). Note that the dimension esu/atom corresponds to cm^5/statvolt.

material	$\chi_{nr,\,opt}$ (10^{-21} m^2/V^2)	$\chi_{nr,\,opt}/N$ (10^{-35} esu/atom)
Al_2O_3	0.31	0.22
diamond	2.5	1.8
CdS	98	70

Table 1. Measured non-resonant third-order susceptibilities for materials at optical wavelengths [10].

We can use the anharmonic oscillator model to estimate the magnitude of $\chi^{(3)}$ for resonant Raman scattering at X-ray energies, by setting $\omega_1 = \omega_0 = \omega_2 + \Omega$ and assuming that the linewidth γ and valence splitting Ω satisfy $\gamma \approx \Omega << \omega_0$. We thus obtain:

$$\mathrm{Im}\left(\chi_{res}^{(3)}\right) / N \approx \frac{e^4}{8\varepsilon_0 m^3 r_a^2 \omega_0^2 \gamma^4} \qquad (4)$$

In order to calculate approximate numerical values, we assume a linewidth $\hbar\gamma = 1$ eV; note the high sensitivity of χ to the exact value of γ. The results are given in Table 2 and compared with more detailed calculations from the literature. The agreement must be regarded as quite acceptable, given the highly approximate nature of the model. Note the similar order of magnitude for the *non-resonant* susceptibility at *optical* frequencies and the *resonant* susceptibility at *X-ray* frequencies.

atom	r_a (Å)	$\hbar\omega_0$ (eV)	$\chi_{res,\,X\text{-}ray}/N$ (10^{-35} esu/atom)	literature value
He	0.31	20.6	232	460 [12]
C	0.7	277	0.25	35 [13]

Table 2. Resonant Raman susceptibilities for atoms at X-ray wavelengths, from the anharmonic oscillator model [10], assuming a 1 eV linewidth, and compared with more detailed calculations from the literature.

The Raman scattering cross-section

The efficiency of a third-order non-parametric process is generally expressed in terms of the differential scattering cross-section $\frac{d^2\sigma}{d\Omega_2 d\omega_2}$, where $d\Omega_2$ and $d\omega_2$ are the solid angle and bandwidth of the outgoing radiation. For the *stimulated* Raman effect, with incident beams at both ω_1 and ω_2, Lee and Albrecht [11] derive the following expression:

$$\frac{d^2\sigma_{stim}}{d\Omega_2 d\omega_2} = \frac{32\pi^2\hbar\omega_1\omega_2}{\varepsilon_0 c^2} F(\omega_2)\,\mathrm{Im}\left(\chi^{(3)}\right)/N \qquad (5)$$

where $F(\omega_2)$ is the incident ω_2 photon flux per unit scattered frequency. As discussed by these authors, a spontaneous emission is identical to a stimulated emission in which the stimulating radiation arises from the zero-point field of the black-body spectrum [14]. (See also a discussion of the Einstein coefficients A and B governing light absorption and emission [15].) The Planck radiation law, which gives the number of emitted photons per second, area, steradian and frequency interval is:

$$F_{BB}(\omega,T) \propto \frac{\omega^2}{c^2}\left(\frac{1}{\exp(\hbar\omega/kT)-1} + \frac{1}{2}\right) \qquad (6)$$

For optical radiation at room temperature, only the zero-point photons are of importance, hence:

$$F_{spon}(\omega_2) = F_{BB}(\omega_2,0) \propto \frac{\omega_2^2}{c^2} \qquad (7)$$

With the correct numerical prefactors, Lee and Albrecht show that:

$$\frac{d^2\sigma_{spon}}{d\Omega_2 d\omega_2} = \frac{\hbar\omega_1\omega_2^3}{\pi\varepsilon_0 c^4}\mathrm{Im}\left(\chi^{(3)}\right)/N \tag{8}$$

We may check this expression for the differential cross-section for spontaneous Raman scattering by comparing it with the typical value $\frac{d\sigma_{spon}}{d\Omega_2} = 2 \times 10^{-35}$ m^2/str/molecule, cited by Devir and Bauer [16] for vibrational Raman scattering with a Ruby laser ($\omega_1 \approx \omega_2 = 2.7 \times 10^{15}$ s^{-1}), a linewidth $\Delta\omega_2 = \gamma = 1.9 \times 10^9$ s^{-1}, and a density $N = 10^{28}$ molecules/m^3. Using the formula from Lee and Albrecht, we then calculate the reasonable susceptibility value Im($\chi^{(3)}$) = 4.2×10^{-21} m^2/V^2.

Consider now the *stimulated* case. According to the arguments above, stimulated Raman scattering will predominate over spontaneous Raman scattering when the incident ω_2 flux exceeds that from the zero-point black-body radiation. Quantitatively, the stimulated and spontaneous Raman cross-sections derived by Lee and Albrecht are equal for

$$F(\omega_2) = \frac{\omega_2^2}{32\pi^3 c^2} \tag{9}$$

which, for a photon energy of 277 eV, a pulse duration of 100 fs, a focus spot of (100 μm)^2 and an XFEL bandwidth in the self-amplyfing spontaneous emission (SASE) mode of 0.5% (= 1.4 eV), corresponds to 4×10^9 photons/pulse, *i.e.*, easily supplied by the LCLS (10^{12} photons/pulse).

The angular distribution of spontaneous Raman scattering reflects the angular momentum of the excitation imparted to the sample. Scattering in a molecular liquid shows a $\cos^2\theta$ dipole radiation pattern or a more complex quadrupole pattern, depending on the point-group symmerty of the molecular transitions [17,18]. Characteristic three-lobed emission patterns are observed for Raman scattering by longitudinal and transverse optical phonons in a cubic crystal [19], and for RIXS, a complex dependence on emission angle, incident and outgoing polarization and resonant energy reflects spin and orbital interactions near the L- and M-edges in transition-metal compounds [20]. *Stimulated* Raman scattering amplifies the ω_2 field only in a narrow cone about the forward and backward [21] directions, with an angular-momentum-dependent gain. The cross-sections cited above refer to the simple case of *s*-wave scattering. An intuitive, mechanical model for resonance stimulated Raman scattering by molecular vibrations has been given by Hemmer and Prentiss [22].

Stimulated emission pumping and stimulated Raman pumping

Stimulated optical emission from a highly-excited state (*e*) has been found to be an efficient method of selectively populating vibrational states (*f*) which, by symmetry, cannot be excited by IR-absorption [23,24] (see Fig. 2). In order to increase the selectivity of the excited low-lying state, such stimulated emission pumping (SEP) is usually performed with sequential ω_1 and ω_2

pulses, rather than simultaneously in a stimulated Raman process. In this case, ω_1 is called the *pump* beam, and ω_2 the *dump* beam. The preferred method to detect SEP is via the accompanying decrease in resonant fluorescence (*fluorescence dip detection*); in order to minimize the effect of pulse-to-pulse intensity fluctuations, the pump beam is split into parallel measurements, one with (*signal*) and one without (*reference*) the dump beam present [24]. The dump wavelength is then scanned until a dip in the normalized fluorescence is observed.

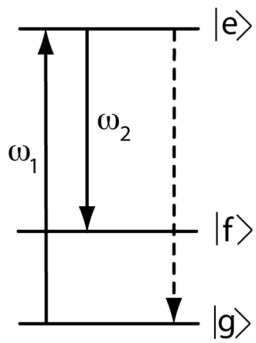

Figure 2. Schematic representation of selective excitation of a level *f* via (sequential) stimulated emission pumping (SEP), and its dectection via a fluorescence dip.

Simultaneous ω_1 and ω_2 pulses can also be used to efficiently pump a low-level excited state, albeit with reduced selectivity. The rate of such stimulated Raman pumping is proportional to the cross-section for spontaneous Raman scattering [16,21]:

$$\begin{aligned}\frac{\partial\Delta}{\Delta} &= \frac{-32\pi^2 c^2 I_1 I_2 \tau}{\hbar^2 c^3 \omega_2^4 \gamma}\left(\frac{d\sigma_{spon}}{d\Omega_2}\right) \\ &\approx \frac{-32\pi I_1 I_2 \tau}{\varepsilon_0 \hbar c^2}\,\mathrm{Im}\left(\frac{\chi^{(3)}}{N}\right)\end{aligned} \tag{10}$$

Here Δ is the fractional ground-state population, and I_1 and I_2 are the intensities of the pump and Stokes pulses, each of duration τ. In the second line of Eq. (10), the expression for the differential Raman cross-section from Eq. (8) was used, and it was assumed that the bandwidth $\Delta\omega_2$ is equal to the Raman linewidth γ. If we take the $\chi^{(3)}$ value from Tanaka and Mukamel for carbon at 277 eV (Table 2) and assume a molecular density $N = 10^{28}$ m^{-3}, a pulse duration $\tau = 20$ fs, a spot size of (100 μm)^2 and equal intensities $I_1 = I_2$, we find that a relative population change $\delta\Delta/\Delta = -1$ is produced by an X-ray power in each beam of 30 MW. Note that the LCLS is capable of 10 GW.

Impulsive stimulated Raman scattering

The frequency-time uncertainty principle states that the minimum time-bandwidth product of an optical pulse is obtained for a gaussian profile:

$$\left(\Delta E \cdot \tau\right)_{\min} = \hbar\Delta\omega_{FWHM}\tau_{FWHM} = 8\hbar\ln 2 = 3.65\ \mathrm{eV\,fs} \tag{11}$$

Thus a single sufficiently short pulse (ω_{imp}) will contain a broad range of spectral components and can be used to simultaneously deliver both the Raman pump (ω_1) and Stokes stimulation (ω_2) waves in a stimulated scattering experiment. This is the concept behind *impulsive stimulated Raman scattering* (ISRS) [25] (see Fig. 3).

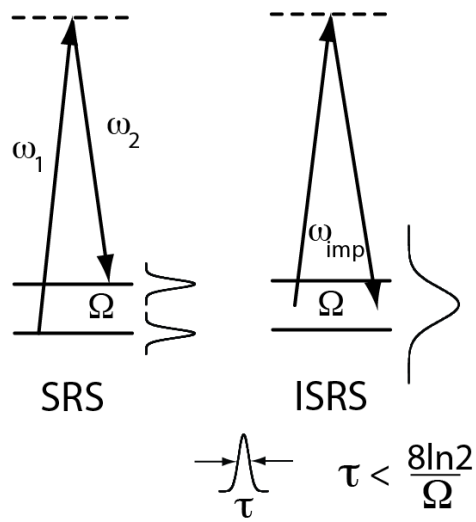

Figure 3. A schematic comparison of stimulated Raman scattering (SRS) and impulsive stimulated Raman scattering (ISRS).

The degeneracy parameter

From the arguments of Lee and Albrecht leading up to Eqn. (9), we expect stimulated Raman scattering to outweigh the spontaneous Raman effect when the incident photon flux exceeds that from the zero-point black-body background, which corresponds, in turn, to one photon per radiation mode. In Bloembergen's words [9], "... *the stimulated effect will only be comparable to or larger than the spontaneous emission if the number of incident photons is so large that it exceeds the number of vacuum electromagnetic modes contained in the frequency interval of the linewidth*." The number of photons per mode for a light source is given by the degeneracy parameter δ. When $\delta >> 1$, the statistical properties of the light source can be treated classically, and when δ is of order or less than unity, quantum statistics are called for [26].

The degeneracy parameter can also be expressed [27] as the number of photons in a coherence volume, given by the lateral coherence area times the longitudinal coherence length. Furthermore, it is related [28] to the source brilliance *Br* (expressed as photons/second/source size/solid angle divergence/bandwidth) according to:

$$\delta = Br \cdot \frac{1}{\pi \Delta \nu} \cdot A_s \cdot \frac{\lambda^2}{A_s} \cdot \frac{\Delta \nu}{\nu} = Br \cdot \frac{\lambda^3}{\pi c} \qquad (12)$$

where $\Delta\nu$ is the source bandwidth, A_s is the source area, and λ is the emission wavelength. For pulsed radiation from the XFEL, Saldin, *et al*. [29] show that δ is given by $\delta = \dot{n}_{ph} \tau_c \varsigma$, where

$\dot{n}_{ph}$ is the number of photons in the pulse divided by the pulse duration, $\tau_c = \sqrt{\pi} / \sigma_\omega$ is the correlation time, which is inversely proportional to the rms SASE bandwidth σ_ω, and ζ is the degree of transverse coherence. The transverse coherence is in turn related to the transverse phase space product (the product of the rms beam waist radius and the rms divergence angle) by $\sigma_r \sigma_\theta = \frac{\lambda}{4\pi\zeta}$, and it is equal to the inverse of the number of effective Hermite modes required to describe the transverse radiation profile. From a simulation based on LCLS parameters, Saldin, *et al.*, predict $\zeta = 0.83$. Values of δ for various sources have been given by Lengeler [27] (see Table 3).

source	photon energy	δ
Hg lamp	4.9 eV	3×10^{-3}
synchrotron undulator	6.4 keV	2×10^{-3}
He-Ne laser	1.96 eV	2×10^{7}
XFEL	6.4 keV	2×10^{9}

Table 3. Estimates of the degeneracy parameter δ for various light sources [27].

As noted by Bloembergen, for the stimulated Raman effect, the relevant degeneracy is that which falls within the Raman linewidth, and the values in Table 3 should be adjusted accordingly. But just as the qualitative step in brilliance from a thermal source to the optical laser opened the field of non-linear optics, one may expect that the similar increase from a synchrotron undulator to the XFEL will mark the beginning of non-linear X-ray optics.

Homodyne *vs.* heterodyne detection

Detection of a scattered signal generally proceeds according to one of two schemes: In radio-frequency technology, *homodyne* detection refers to mixing the perturbed signal to be detected with a reference which has been derived from the signal prior to perturbation, and in *heterodyne* detection, the reference is produced by an independent *local oscillator*. Since phase stablility is generally not achievable with independent optical sources, the terms homodyne and heterodyne have a different meaning in optics (see Fig. 4). Here *homodyne* refers to the direct detection with a square-law detector of a signal ω_s, yielding the intensity I_{hom}, which is proportional to the modulus squared of the susceptibility χ times the initial intensity I_0. This detection method has the advantages of simplicity and low background.

In *heterodyne* optical detection, on the other hand, part of the incoming beam ω_0 is split off as an (intense) reference and mixed at the detector with the (weak) signal ω_s. The resulting intensity I_{het} now has a contribution which is proportional to $\chi E_0 E_s$. By varying the relative phase of reference and signal, it is in principle possible to separately determine the real and imaginary parts of χ, although this is problematic at X-ray wavelengths. The advantage of heterodyne detection is that the interference signal can in principle, by increasing the reference intensity, be made arbitrarily large, but this will also increase the background. Note that if the detector has sufficient bandwidth, the inelastic frequency difference ω_s- ω_0 will be resolved as heterodyne beating.

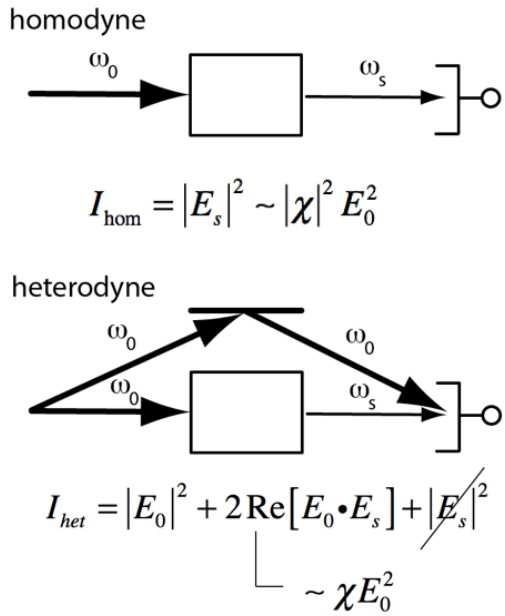

Figure 4. Homodyne *vs*. heterodyne optical detection, illustrated for the case of a linear optical response. Note that the signal *s* has as its source the electric polarization χE_0.

Parametric spectroscopy

The prime example of 3rd order parametric optical spectroscopy is four-wave mixing (see Fig. 5), in which three incident waves ω_1, ω_2 and ω_0 generate an (*anti-Stokes*) signal wave ω_s, which is either directly homodyne detected or mixed with a heterodyne reference wave. A variation on this method is *degenerate* four-wave mixing, in which all four waves have the same frequency, and which is used, for example, in phase-conjugate mirrors [10,30]. Two four-wave mixing schemes which may lend themselves to time-resolved X-ray spectroscopy are time-resolved CARS (coherent anti-Stokes Raman scattering) and 2-dimensional correlation spectroscopy. Note that the term *coherent* implies that the probability for the process is given by the square of the sum of probability amplitudes describing alternate paths to the same result.

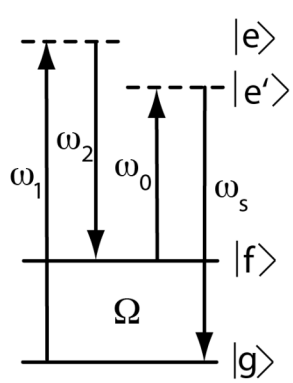

Figure 5. The generic parametric four-wave mixing scheme.

Time-resolved CARS (see Fig. 6) is an established method in optical spectroscopy [31]. A stimulated Raman scattering (ω_1, ω_2), or alternatively, a sufficiently short impulsive stimulation, is used to prepare a coherent superposition of low-lying excited states *f*, and after a time delay τ, this superposition is queried by a second ω_1 pulse, which produces the homodyne-detected anti-Stokes signal ω_s. Since the superposition of states *f* will evolve during the delay, quantum-beats at the *f*-state splitting $\delta\Omega$ will be detected as τ is varied. This is the basis of the *coherent X-ray scattering* method proposed by Tanaka and Mukamel [13].

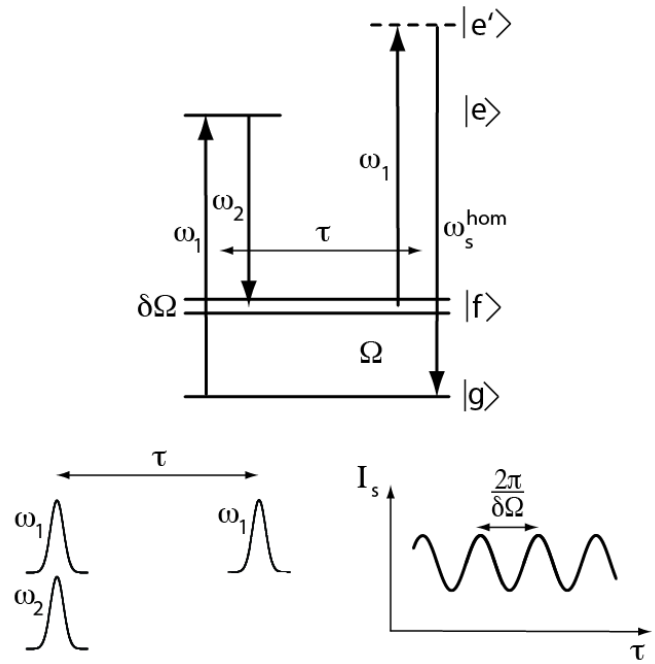

Figure 6. The time-resolved coherent anti-Stokes Raman scattering (CARS) technique.

A still more ambitious time-resolved non-linear X-ray spectroscopy, analogous to multi-pulse NMR, is the *2-d X-ray correlation spectroscopy* proposed by Mukamel, *et al*. [32] (see Fig. 7). In this four-wave mixing experiment, coherent excitation of short-lived (fs), localized core-excited states, for example, on different atomic species (N and O) within the same molecule, allows one to study the correlation and dynamics of highly-excited wavepackets. It should be noted that as in t-resolved CARS, in spite of the use of short, spectrally-broad pulses, high spectral resolution is achieved via Fourier analysis, in this case with respect to the two inter-pulse delays τ_1 and τ_3. The method requires precise timing of sub-fs pulses.

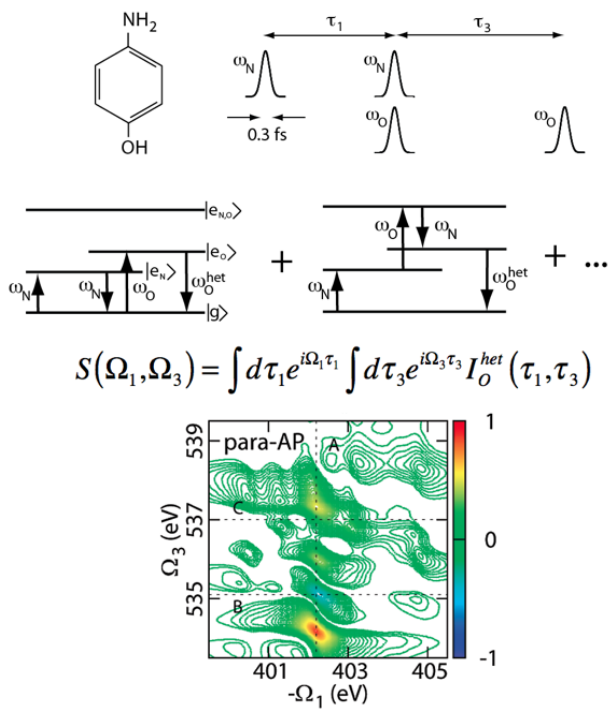

Figure 7. The proposed 2-d X-ray correlation spectroscopy technique [32]. A two-dimensional Fourier analysis with respect to the inter-pulse delays τ_1 and τ_3 yields detailed information on the interference of different core-excitation pathways.

Phase-matching

Energy conservation, which is implicit in the total energy diagrams we have used to describe non-linear optical spectroscopies, assures that the temporal phases of the interacting light waves are matched. A similar requirement on the spatial phase requires momentum conservation, which in practise can be used to provide angular discrimination of a weak signal beam. In a non-parametric interaction, momentum conservation also determines the wave-vector $\vec{q}$ of the excitation undergone by the sample.

Schematic phase-matching conditions are shown in Fig. 8 for a variety of non-linear spectroscopies [30]. In the upper part of the Figure, planar arrangements for the interacting wave-vectors are illustrated for stimulated Raman scattering (SRS) (where an incoming photon $\vec{k}_1$ is converted into an outgoing photon $\vec{k}_2$, causing a sample excitation $\vec{q}$), four-wave mixing (FWM) and coherent anti-Stokes Raman scattering (CARS) (where three incoming waves add to produce the outgoing wave $\vec{k}_s$), and transient-grating spectroscopy (TGS) (see the following Section). In the lower part of the Figure, the BOXCARS configuration [33] for FWM is shown, where the four waves interact in three dimensions. At optical wavelengths, the two dotted squares represent convex lenses, with the sample at their focii.

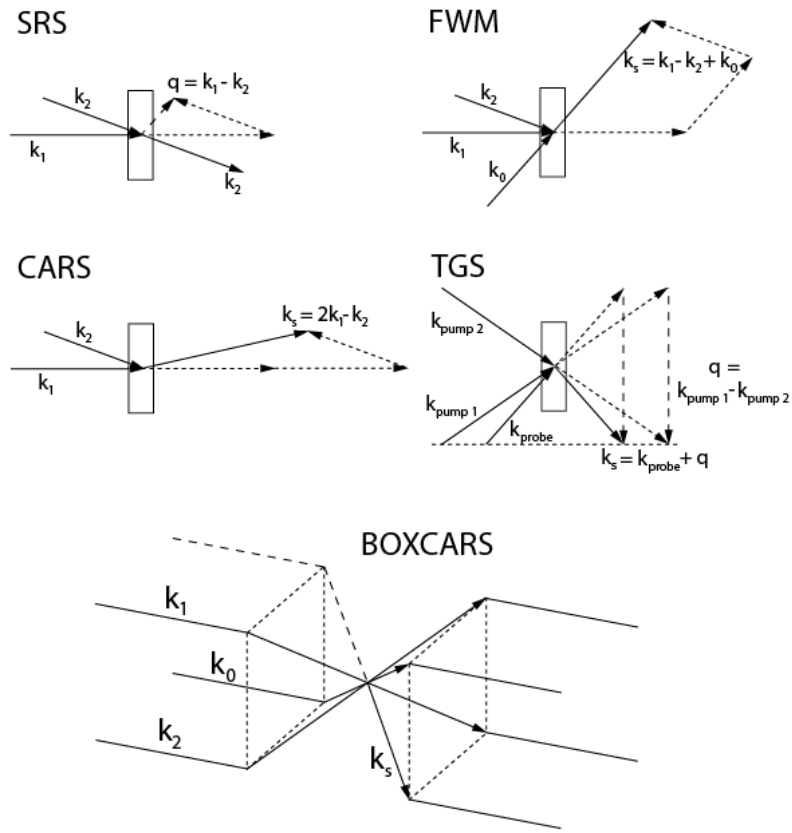

Figure 8. Planar and 3d configurations which assure spatial phase matching in various non-linear optical spectroscopies.

Transient grating spectroscopy

An elegant method of detection for transient optical effects, which allows direct control over the wave-vector $\vec{q}$ of the excitation and spatial discrimination of the signal wave, is *transient grating spectroscopy* (TGS) [34,35]. The principle of TGS is that a pump pulse is split and the two halves are recombined at the sample under a relative angle θ, to produce a standing wave of periodicity $D = 2\pi/q = \lambda_{pump}/2\sin\theta$ (Figs. 8 and 9). Interaction of the standing wave with the sample generates an oscillating, spatially-periodic distribution of excitation in the form of a transient grating, which survives for the lifetime of the excitation. A delayed probe pulse is then diffracted by the grating and measures its strength after a delay τ. One can use an impulsive excitation pulse, which pumps the sample via stimulated Raman pumping, followed by a probe pulse, which queries the sample via four-wave mixing. Then the Raman gain in effect redirects a photon from one of the pump beams into the other.

A proposed geometry for a soft X-ray TGS experiment based on transmission diffraction gratings is shown in Fig. 9 [36,37]; the setup guarantees that regardless of the probe wavelength, the Bragg condition will be satisfied for diffraction by the transient grating D. For concreteness, we consider a stimulated RIXS measurement with the pump pulse at the copper L_2-edge (952 eV) and the probe pulse at the L_3-edge (933 eV). Such a measurement could be sensitive to *e.g.*

collective spin excitations in the correlated electron material $Sr_{14}Cu_{24}O_{41}$ [5]. Free-standing diamond gratings, with 300 nm ridges on 3 μm thick substrates and with coarse and fine periods d = 340 and $d/2$ = 170 nm, will each have 7% transmission [38]. And they will produce pump and probe deflection angles $\theta = 0.22^{o}$ and $\theta' = 0.25^{o}$ with a 1st order diffraction efficiency of 12%, for a total transmission to the sample of 7×10^{-5}. The small deflection angle implies that a large separation is needed between the two gratings, in order to selectively block probe pulses which would otherwise enter the detector; at 1 m separation, the pump and probe beams at grating 2 will be displaced from one another by only 90 μm. The energy of the spin excitations is approximately 200 meV, so a transform-limited pulse will have to be shorter than 15 fs in duration for impulsive stimulated pumping. A primary concern, of course, will be the production of suitably delayed two-color pulses; several multi-wavelength XFEL modes are under consideration for LCLS-II [7]. It should be noted that soft X-ray optical split-and-delay units must use diffraction gratings or glancing-incidence mirrors [39] and hence will be limited to delays below a few ps.

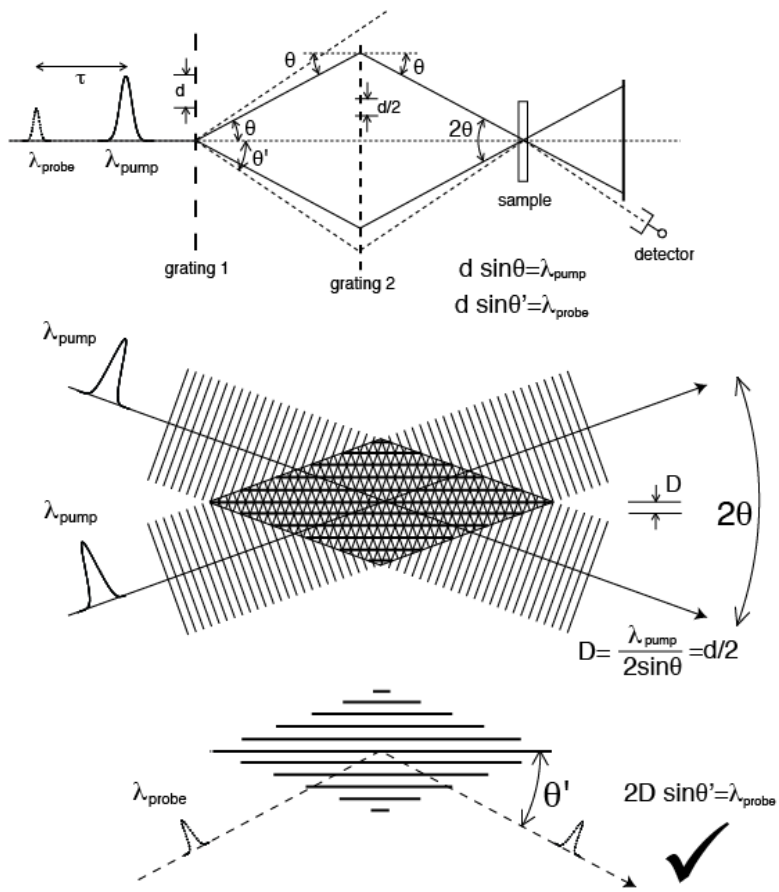

Figure 9. Diffraction-based geometry for transient grating spectroscopy [36].

An alternative XFEL-based TGS methodology would be used for hard X-ray spectroscopy, with which, for example, collective magnetic excitations in La_2CuO_4 could be studied at the copper K-edge (8.98 keV) [4]. With hard X-rays, it is feasible to use crystals to split and redirect the XFEL pulses [40]. A possible experimental geometry, including an energy selective split and delay unit, is shown in Fig. 10. Two-color pulses are incident from the left, and the three silicon crystals S_1,

S_2 and S_3 constitute the tunable split-and-delay unit, with a maximum delay of several ns and an overall transmission of approximately 1%. Situated at a different Bragg angle, the crystals G_1, G_2 and G_3 generate from the pump pulse a transient grating in the sample, with the same lattice spacing and orientation as those of the crystals, by which the delayed probe pulse is diffracted into the detector. The crystals S_1 and G_1 are sufficiently thin (30 μm) to allow substantial transmission (75%). It may be advantageous to machine the G-crystals from a monolithic substrate. The 0.014% Darwin width of the Si [111] reflection, corresponding to 1.3 eV, and a the use of a 7 fs transform-limited pulse will allow impulsive pumping of the 500 meV excitations.

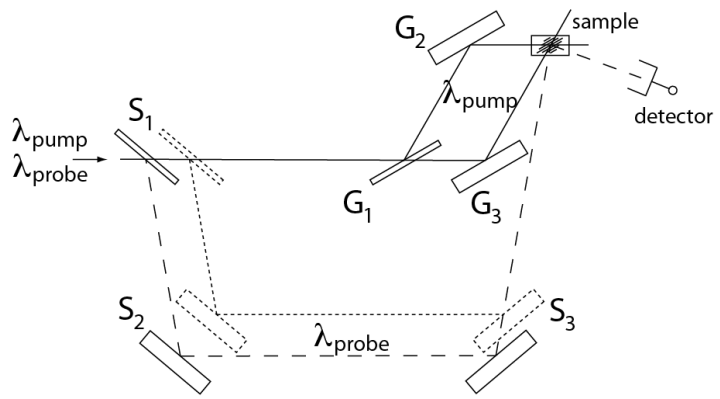

Fig. 10. A schematic hard-X-ray transient-grating geometry, based on the use of diffracting crystals. Two positions of the S-crystals are shown, corresponding to different pump-probe delays.

Conclusions

Will stimulated resonance X-ray Raman scattering, perhaps with two-color excitation/detection, become a routine method of performing time-resolved inelastic X-ray spectroscopy at an XFEL such as the LCLS? This is a non-trivial question, and without detailed simulations, or better, clear experimental evidence, only plausibility arguments can be put forward.

There is preliminary evidence that *elastic* stimulated X-ray scattering in an atomic system has already been observed at the LCLS. In an internal report on their beamtime at the AMO station in October-November, 2009 [41], an experimental team from Argonne National Laboratory suggests that they have seen evidence of Rabi flopping, a stimulated process in which a two-level quantum system is coherently driven up and down in energy: upon resonantly exciting the 849 eV 1s→2p transition in Ne, a line-broadening was observed at high fluence, indicating a reduced excited state lifetime, which is in qualitative agreement with theory [42]. The data are yet to be published.

The most detailed theoretical predictions of stimulated X-ray scattering performed to date are quite optimistic. In gaseous helium, Fill, *et al.*, [12] have predicted that a high stimulated Raman gain can be achieved with an intensity of 60 eV pump radiation of 10^{11} W/cm^2 (corresponding to a 100 fs pulse of 10^{11} photons into a (100 μm)^2 spot - see also Table 2). And in gaseous argon, Sun, *et al.*, [43] predict the appearance of a strong Stokes signal from a 6 fs pulse of 244 eV pump radiation containing 2×10^{13} photons in a (100 μm)^2 spot. In a model organic molecular

solid, Tanaka and Mukamel [13], on the basis of a detailed evaluation of $\chi^{(3)}$ for the carbon 1s→2p transition at 277 eV (see Table 2), state that coherent X-ray Raman spectroscopy at an XFEL is feasible. In a more general vein, the concluding remarks of a paper on optical scattering [44] state: "S*timulated Raman scattering must occur whenever a suffciently short light pulse passes through any Raman-active medium, resulting in coherent excitation of the medium and spectral changes in the pulse. Impulsive stimulated Raman scattering is therefore a general aspect of the way in which an ultrashort light pulse interacts with matter.* "

Of importance for a successful XFEL-based X-ray pump / X-ray probe technique are the inter-related issues of sample damage and signal-to-noise ratio. Since stimulated Raman scattering has no threshold, with sufficient discrimination against background effects such as elastic scattering, incoherent fluorescence and non-radiative transitions, one needs only to collect data from a sufficient number of unfocused and/or attenuated XFEL pulses to guarantee statistical significance. Although pilot experiments with various measurement geometries and on different model systems are clearly called for, the simplicity and high potential for spectral and wave-vector discrimination inherent in the transient grating approach make this technique a prime contender.

Consider how a TGS experiment at an XFEL would function: Light-sample interactions other than impulsively stimulated Raman scattering can produce a spatial modulation of the refractive index of the sample and hence a transient grating, but as the pump fluence is increased, stimulated processes may be expected to dominate. However, increased fluence, particularly when close to resonance absorption, brings with it the danger of optical damage by photochemistry, local heating or even surface ablation. Thus the sample properties and X-ray fluence must be carefully chosen to avoid unwanted complications. It is necessary that the pump and probe wavelengths be different enough to allow angular discrimination of the diffracted probe beam. This is because, for a typical pump-probe delay below a nanosecond, it will generally not be possible to discriminate the pulses on the basis of their arrival times. Furthermore, a two-color experiment can offer improved selectivity in controlling the light-matter interaction [45]. It must be remembered, however, that a FWM interaction requires significant optical non-linearity, implying that also the probe wavelength should lie in the vicinity of an electronic resonance. We have seen that impulsive stimulation of a Raman process requires a sufficient frequency bandwidth for the pump pulse. The intrinsic lifetime broadening of the pulse may be enhanced by the chaotic SASE process itself and may be further increased by an energy chirp of the XFEL beam. An increased bandwidth may, however, place restrictions on the bandpass of the gratings or crystals used.

On a more fundamental level, since a time-dependent observation can be regarded as the Fourier transform of a spectral measurement, one may ask what information can an XFEL-based, transient grating spectroscopy experiment deliver which is inaccessible to a synchrotron-based RIXS measurement. The answer probably lies in short-lived, diffusive phenomena, which appear as broad structureless bumps in a frequency spectrum but which exhibit characteristic waveforms in the time domain. Examples of such phenomena are the fluctuations of charge, spin and orbital order which are believed to play an intrinsic role in correlated electron materials [46].

Acknowledgements

The author wishes to acknowledge highly informative discussions with the following individuals: Don Bethune, Sebastian Doniach, Shaul Mukamel, Zahid Hussain, Bill McCurdy, Ali Belkacem, Z-X Shen, Keith Nelson, Michael Rowen, Yiping Feng, Harry Ihee, Jan Feldkamp and Uwe Bergmann. Special thanks to go the initiator and strong supporter of this work, Jerry Hastings.

References

* email address: *bruce.patterson@psi.ch*

[1] M Altarelli, *Resonant x-ray scattering: a theoretical introduction*, Lecture Notes in Physics, **697**, 201-242 (2006).

[2] JE Rubensson, *RIXS dynamics for beginners*, J. El. Spect. Rel. Phenom. **110-111**, 135-151 (2000).

[3] MZ Hasan, *et al.*, *Electronic structure of Mott insulators studied by inelastic X-ray scattering*, Science **288**, 1811-1814 (2000).

[4] JP Hill, *et al.*, *Observation of a 500 meV collective mode in* $La_{2-x}Sr_xCuO_4$ *and* Nd_2CuO_4 *using resonant inelastic X-ray scattering*, Phys. Rev. Lett. **100**, 097001 (2008).

[5] J Schlappa, *et al.*, *Collective magnetic excitations in the spin ladder* $Sr_{14}Cu_{24}O_{41}$ *measured using high-resolution resonant inelastic X-ray scattering*, Phys. Rev. Lett. **103**, 047401 (2009).

[6] https://slacportal.slac.stanford.edu/sites/lcls_public/

[7] https://slacportal.slac.stanford.edu/sites/lcls_public/lcls_ii/

[8] S Mukamel and S Rahav, *Ultrafast nonlinear optical signals viewed from the molecule's perspective; Kramers-Heisenberg transition amplitudes vs susceptibilities*, submitted (2010).

[9] N Bloembergen, *The stimulated Raman effect*, Am. J. Phys. 35, 989-1023 (1967); *Nonlinear optics and spectroscopy*, Science **216**, 1057-1064 (1982).

[10] RW Boyd, *Nonlinear Optics*, Elsevier, (2008).

[11] D Lee and AC Albrecht, *A unified view of Raman, resonance Raman and fluorescence spectroscopy*, Adv. IR and Raman Spect., *ed*. RJH Clark and RE Hester, Wiley, **12**, 179-213 (1985).

[12] EE Fill, *et al.*, *Stimulated Raman scattering in helium with soft x-ray laser radiation*, Phys. Rev. A **54**, 5374-5377 (1996).

[13] S Tanaka and S Mukamel, *Coherent X-ray Raman spectroscopy: a nonlinear local probe for electronic excitations*, Phys. Rev. Lett. **89**, 043001 (2002).

[14] J Mehra and H Rechenberg, *Planck's half-quanta: a history of the concept of zero-point energy*, Found. Phys. **29**, 91-132 (1999).

[15] W McCrea, *Time, vacuum and cosmos*, Quart. J. Roy. Astr. Soc. **27**, 137-152 (1986).

[16] AD Devir and SH Bauer, *Vibration relaxation time measurement via coherent Raman induced infrared fluoresence*, J. Chem. Phys. **69**, 2682-2687 (1978).

[17] TC Damen, RCC Leite and SPS Porto, *Angular dependence of the Raman scattering from benzene excited by the He-Ne cw laser*, Phys. Rev. Lett. **14**, 9-11 (1965).

[18] L Nafie, P Stein, B Fanconi and WL Peticolas, *Angular dependence of Raman scattering intensity*, J. Chem. Phys. **52**, 1584-1588 (1970).
[19] P Dawson, *Anisotropy of Raman scattering in a cubic crystal*, J. Opt. Soc. Am. **62**, 1049-1051 (1972).
[20] M van Veenendaal, *Polarization dependence of L- and M-edge resonant inelastic X-ray scattering in transition-metal compounds*, Phys. Rev. Lett. **96**, 117404 (2006).
[21] M Maier, W Kaiser and JA Giordmaine, *Backward stimulated Raman scattering*, Phys. Rev. **177**, 580-599 (1969).
[22] PR Hemmer and MG Prentiss, *Coupled-pendulum model of the stimulated resonance Raman effect*, J. Opt. Soc. Am. B **5**, 1613-1623 (1988).
[23] AE DePristo, H. Rabitz and RB Miles, *The selective preparation of excited vibrational states using the stimulated resonance Raman effect*, J. Chem. Phys. **73**, 4798-4806 (1908).
[24] C. Kittrell, *et al.*, *Selective vibrational excitation by stimulated emission pumping*, J. Chem. Phys. **75**, 2056-9 (1981).
[25] Y Yan and KA Nelson, *Impulsive stimulated light scattering. I. General theory*, J. Chem. Phys. **87**, 6240-6258 (1987).
[26] JW Goodman, *Statistical Optics*, Wiley (1985).
[27] B Lengeler, *Coherence*, www.institut2b.physik.rwthaachen.de/vorlesung/COHERENCE.pdf
[28] B Lengeler, *Coherence in X-ray physics*, Naturwissenschaften **88**, 249-260 (2001).
[29] EL Saldin, EA Schneidmiller and MV Yurkov, *Coherence properties of the radiation from X-ray free electron laser*, Opt. Comm. **281**, 1179-1188 (2008).
[30] CW Thiel, *Four-wave mixing and its applications*, http://www.physics.montana.edu/students/thiel/docs/FWMixing.pdf
[31] W Kiefer, A Materny and M Schmitt, *Femtosecond time-resolved spectroscopy of elementary molecular dynamics*, Naturwissenschaften **89**, 250-258 (2002).
[32] S Mukamel, *et al.*, *Coherent multidimensional optical probes for electron correlations and exciton dynamics: from NMR to X-rays*, Accounts Chem. Res. **42**, 553-562 (2009).
[33] D Romanov, A Filin, R Compton and R Levis, *Phase matching in femtosecond BOXCARS*, Opt. Lett. **32**, 3161-3163 (2007).
[34] MD Fayer, *Dynamics of molecules in condensed phases: picosecond holographc grating experiments*, Ann. Rev. Phys. Chem. 3**3**, 63-87 (1982).
[35] M Motzkus, S Pedersen and AH Zewail, *Nonlinear (DFWM) techniques for probing transition states of uni- and bimolecular reactions*, J. Phys. Chem. **100**, 5620-5633 (1996).
[36] DE Moncton, *X-ray laser user facility at Bates laboratory*, filburt.mit.edu/xfel/fel_files/nsfproposal.pdf (2003).
[37] G Dadusc, *et al.*, *Diffractive optics-based heterodyne-detected four-wave mixing signals of protein motion*, PNAS **98**, 6110-6115 (2001).
[38] Center for X-ray Optics, *X-ray interactions with matter*, http://henke.lbl.gov/optical_constants/
[39] R Mitzner, *et al.*, *Spatio-temporal coherence of free electron laser pulses in the soft x-ray regime*, Opt. Expr. **16**, 19909-19919 (2008).
[40] W Roseker, *et al.*, *Performance of a ps x-ray delay line unit at 8.39 keV*, Opt. Lett. **34**, 1768-1770 (2009).

[41] B Krässig, *AMO adventures at the LCLS*, http://www.aps.anl.gov./News/Meetings/Monthly_Meetings/2009/Presentations/2091216_krassig.pdf
[42] N Rohringer and R Santra, *Resonant Auger effect at high x-ray intensity*, Phys. Rev. A **77**, 053404 (2008).
[43] YP Sun, JC Liu, CK Wang and F Gel'mukhanov, *Propagation of a strong x-ray pulse: pulse compression, stimulated Raman scattering, amplified spontaneous emission, lasing without inversion, and four-wave mixing*, Phys. Rev. A **81**, 013812 (2010).
[44] S Ruhman, *et al*., *Intramolecular and intermolecular dynamics in molecular liquids through femtosecond time-resolved impulsive stimulated scattering*, Revue Phys. Appl. **22**, 1717-1734 (1987).
[45] K Kwak, *et al*., *Two-color transient grating spectroscopy of a two-level system*, Bull. Korean Chem. Soc. **24**, 1069-1074 (2003).
[46] E Dagotto, *Complexity in strongly correlated electronic systems*, Science **309**, 257-262 (2005).